Membrane Adsorbents Comprising Self-Assembled Inorganic Nanocages (SINCs) for Super-fast Direct Air Capture Enabled by Passive Cooling

Final Report
Project Period: 10/1/2020 – 12/31/2022

by

Haiqing Lin, Ph.D. and Professor
haiqingl@buffalo.edu
716-645-1856

Date Issued: April 3, 2023

The U.S. Department of Energy
Office of Fossil Energy,
National Energy Technology Laboratory
Award Number: DE-FE0031960

Department of Chemical and Biological Engineering
University at Buffalo, The State University of New York (UB)

Other Contributors:

University at Buffalo

Vinh Bui	Krista Clark	Timothy Cook
Matthew Crawley	Qiaoqiang Gan	Amanda Grass
Leiqing Hu	Jacob Rada	Thien Tran
Heshali Welgama	Dylan Tua	Lyu Zhou

Trimeric Corporation

Andrew Sexton	Clay Jones

DISCLAIMER

Final Report

Covering Period: 10/1/2020 – 12/31/2022
Date Submitted: March 30, 2023
Updated version: April 3, 2023

Federal Agency:	U.S. Department of Energy, National Energy Technology Laboratory
Award Number:	DE-FE0031960
Project Title:	Membrane Adsorbents Comprising Self-Assembled Inorganic Nanocages (SINCs) for Super-fast Direct Air Capture Enabled by Passive Cooling
Technical Contact:	Dr./Prof. Haiqing Lin; haiqingl@buffalo.edu; 716-645-1856
Recipient Organization:	The Research Foundation for State University of New York 402 Crofts Hall, Buffalo, NY 14260
Project Period:	10/1/2020 – 12/31/2022
Signature:	
DOE Project Officer:	Dr. Elliot Roth U.S. Department of Energy National Energy Technology Laboratory 626 Cochran Mill Road 412-386-7314 Elliot.Roth@netl.doe.gov
DOE Contract Specialist:	Caitlin Lecker U.S. Department of Energy National Energy Technology Laboratory 626 Cochrans Mill Road 412-386-9427 Caitlin.Lecker@netl.doe.gov

TABLE OF CONTENTS

1. Executive Summary

The objectives of the proposed project were to develop highly porous membrane adsorbents comprising CO_2-philic polymers and self-assembled inorganic nanocages (SINCs) for rapid temperature swing adsorption using electricity-free solar heating and radiative cooling, enabling an economically viable approach for direct air capture (DAC). Our core technical activities combine three key innovations. (1) Highly porous flat-sheet membrane adsorbents contain CO_2-philic amines that can be easily produced using a phase inversion method. (2) CO_2-philic SINCs can be easily dispersed in the polymers with great stability (compared with the metal-organic frameworks or MOFs). (3) The adsorption and desorption are integrated with solar heating and radiative cooling for rapid continuous operation, in contrast to traditional long-cycle separate operation. The membrane adsorbents containing amines, polymers, and SINCs were produced using a one-step industrial process. The porous membranes coupled with porous SINCs offer low resistance for gas flow and fast CO_2 sorption/desorption cycles, while the incorporation of the additional amine groups provides high CO_2 sorption capacity.

The key achievements are summarized below.

- Membrane adsorbents with high PEI loading (>40%), high porosity of >80%, and low gasflow resistance were prepared in one step using commercially available, low-cost materials
- Membrane adsorbents based on Solupor and PEI show CO_2 sorption capacity of >1.5 mmol/g using air containing 400 ppm at a relative humidity of 15%.
- Effect of the adsorbent compositions (such as PEI type, PEI content, SINC content, porosity) on the CO_2 sorption was systematically investigated.
- Effect of the processing conditions (such as CO_2 content, temperature, and relative humidity) on the CO_2 sorption was systematically investigated;
- The stability of the membrane adsorption against many cycles of sorption and desorption was studied. The higher molecular weight of PEI (PEI25k) shows better stability than PEI800.
- Advanced materials with radiative cooling were developed, which can decrease the temperature by 5-7 ℃ compared to the ambient temperature.
- Preliminary techno-economic analysis shows that our process may achieve a capture cost of \$1,343/tonne CO_2 with a total OPEX cost of \$1,112/tonne CO_2. The adsorbent replacement cost accounted for 52% of the total OPEX cost. Membrane adsorbents with lower costs and longer operation life can significantly decrease the cost.

The proposed project directly addresses the requirement of DE-FOA-0002188, i.e., novel materials with CO_2 adsorption capacity for direct air capture with integrated solar heating and radiative cooling to reduce the cost of the DAC. Our future work will focus on the development of low-cost adsorbents that can be stable at the sorption and desorption conditions for long term.

2. Introduction and Our Approach

2.1. Current Technologies for Direct Air Capture (DAC)

Direct air capture (DAC) has emerged as a critical component in the future energy infrastructure.[1-8] When coupled with hydrogen from electrolysis based on solar energy, the DAC enables flexible production of hydrocarbon fuels or other chemicals.[4, 5, 9] Additionally, the DAC directly reduces the CO_2 content and ultimately mitigate the long-lasting effect of the CO_2 in the atmosphere. The main challenge to the DAC is the low CO_2 content and thus associated high cost.[4, 10, 11] For example, the CO_2 content in the air is 300 times more dilute than in coal-fired power plant flue gas (~12%).

The state-of-the-art technology for DAC is based on sorbents, such as aqueous hydroxide solutions and solid amine sorbents.[8, 11-13] The hydroxide solutions react with CO_2 and achieve high capacity for CO_2 absorption. However, the sorbent regeneration can be costly due to the heating and water evaporation. For example, Carbon Engineering is conducting a pilot-scale test of capturing 1 ton/day CO_2 from the air using liquid KOH solutions.[4] The CO_3^{2-} is then precipitated by reaction with $Ca(OH)_2$, which regenerates KOH and produces $CaCO_3$ for calcination to produce CaO and CO_2. The drying, heating, and calcination (at ~670 °C) is energy-intensive, leading to an energy cost of 8.81 GJ of natural gas per ton CO_2 captured.[4]

Solid sorbents offer the possibility of low energy input, low operating costs, and good scalability.[4] Several companies such as Climeworks, Global Thermostat, Infinitree, and Skytree are developing solid sorbents for CO_2 capture. Amines remain the key groups to be incorporated in the sorbents and tailored for CO_2 capture, as physisorbents (including active carbon, zeolites, and metal-organic frameworks or MOFs) do not show high CO_2 sorption from air. Equations 1 and 2 elucidate the reaction mechanism between the primary and secondary amines and CO_2. Under dry conditions, these amines react with CO_2 and form ammonium carbamate.[13, 14] The maximum molar CO_2/N ratio can be as high as 0.5.

$$CO_2 + 2RNH_2 \leftrightarrow RNH_3^+ + RNHCOO^- \quad (1)$$

$$CO_2 + 2R_1R_2NH \leftrightarrow R_1R_2NH_2^+ + R_1R_2NCOO^- \quad (2)$$

$$CO_2 + R_1R_2NH + H_2O \leftrightarrow R_1R_2NH_2^+HCO_3^- \quad (3)$$

$$CO_2 + R_1R_2R_3N + H_2O \leftrightarrow R_1R_2R_3NH^+HCO_3^- \quad (4)$$

The maximum molar CO_2/N ratio can be increased to 1.0 in the presence of moisture, as shown in Equation 3. Equation 4 shows that water is required for a tertiary amine to react with CO_2.[15] The regeneration of these amine-based sorbents can be at ~ 100 °C, much lower than the hydroxide solutions, leading to potentially lower energy consumption.

Amine groups can be incorporated into solid sorbents in three ways.[12, 13, 16] First, small molecules of amines can be physically impregnated into porous support.[17] However, amines can fill up the pores, creating resistance for the CO_2 to diffuse and react with the amines.[18, 19] More importantly, the amines may be leached during the operation.[20, 21] Second, the amines can be chemically grafted onto the support surface to avoid the amine leaching.[22, 23] The challenge is to increase the grafting density of the amines to improve the CO_2 sorption capacity. Third, the amines can be grafted on the support surface via in situ polymerization to control the grafting density.[24-26] However, this increases the cost of the sorbents. Different approaches can also be combined to increase the amine content and stability.[27]

A variety of solid supports have been explored to incorporate amines (including silica, SBA-15, γ alumina, MCM-41, and MCM-48) and show high CO_2 sorption (1 – 3 mmol/g) from simulated air, as shown in Table 1.[28-32] The sorption is often subject to the slow kinetics due to the CO_2 diffusion. For example, CO_2 sorption in the PEI-modified silica is higher at 75 °C than 25 °C

because of the faster diffusion at 75 °C.[18, 32] The strong interactions between amines and CO_2 may retard the CO_2 diffusion at low temperatures.[33] To this end, MOFs with well-controlled pore size and high porosity have attracted significant attention.[28-32] For example, Mg_2(dobpdc) was doped with N,N′-dimethylethylenediamine (mmen) and show CO_2 sorption comparable to the best results for amines on tailored supports. More importantly, the Mg_2(dobpdc)–mmen show three times faster CO_2 sorption than the amine-functionalized silica.[34]

Table 1. Effect of the amine functionalization of porous supports on the CO_2 sorption capacity from simulated air containing ≈ 400 ppm CO_2.

Porous supports	Temp. (°C)	Relative humidity (%)	CO_2 (mmol/g)	Amine-functionalized	
				Amine type (wt%)	CO_2 (mmol/g)
Fume silica[32]	75	0	0.61	PEI(30)	3.0
SBA-15	75	0		PEI(30)	3.0
γ alumina[35]	30	50		PEI-800(23)	1.7
MIL-101(Cr)[28]	25	0	~0.05	PEI-800(60)	1.3
Mg_2(dobpdc)[34]	25	0		mmen	2.0

As significant attention is dedicated to the solid sorbents with high CO_2 sorption capacity, other characteristics should be obtained for the economically viable DAC, including low cost, long operation life, and excellent manufacturing capability on a large scale. Another critical aspect is to package the sorbents with a low resistance to the airflow, particularly because of the low CO_2 content in the air and the enormous amount of airflow to be processed. Additionally, the energy consumption for the CO_2 desorption needs to be reduced. This project addressed these issues.

2.2. Approach, Rationale, and Preliminary Data for Membrane Adsorbents

The objectives of the proposed project were to develop highly porous membrane adsorbents comprising CO_2-philic polymers and self-assembled inorganic nanocages (SINCs) with a low resistance to airflow and heat transfer for rapid temperature swing adsorption of CO_2 from the air, enabled by electricity-free solar heating and radiative cooling. Our core technical activities combine three key innovations. (1) Highly porous flat-sheet membrane adsorbents contain CO_2-philic amines that can be easily produced using a phase inversion method. (2) CO_2-philic SINCs can be easily dispersed in the polymers with great stability (compared with the MOFs). (3) The adsorption and desorption are integrated with solar heating and radiative cooling for rapid continuous operation, in contrast to traditional long-cycle separate operation. The membrane adsorbents containing amines, polymers, and SINCs can be produced using a one-step industrial process. The porous membranes coupled with porous SINCs offer low resistance for airflow and fast CO_2 sorption/desorption cycles, while the incorporation of the additional amine groups provides high CO_2 sorption capacity.

2.2.1. Overall Process

Figure 1 shows the integrated membrane adsorbents and cooling technology into a single portable system to realize continuous and rapid CO_2 production. A thin sorbent membrane (e.g. 20-100 μm thick) is continuously rotated by a cylinder. The thin film at the bottom of the cylinder can reach saturation within 5 minutes (i.e., adsorption (A)) due to the rapid CO_2 and thermal transport within this thin film into the pores. The use of SINCs instead of MOFs enables the active sorbent sites to be highly dispersed and eliminates the need for the pore-to-pore diffusion that

limits cycling time in MOFs. The CO_2 will be released at the top side of the cylinder (i.e. the desorption process, D, at the temperature of 65~100 ℃) also within 5 minutes by the heater illuminated by a concentrated solar beam or battery-driven heater during nighttime. The obtained CO_2 can be used for algae culturing or greenhouse or further purification. Afterward, the adsorbents will be cooled by topology-optimized convection and radiative cooling structure to accelerate the cycle and improve the sorption capacity.

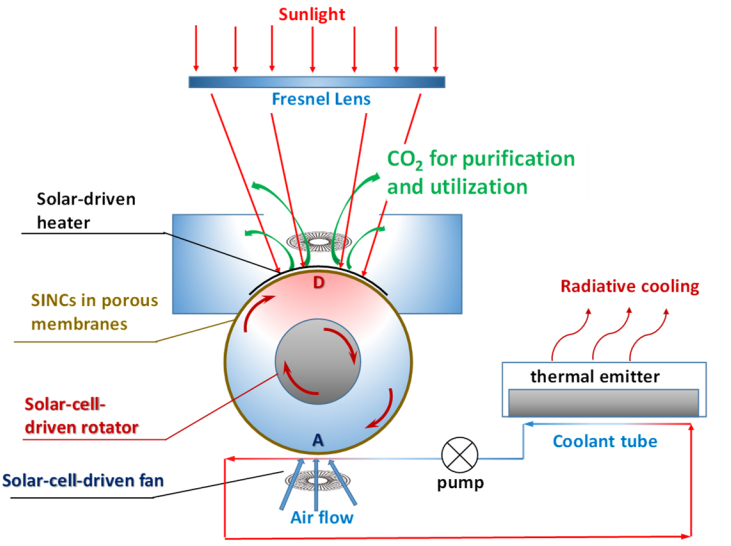

Fig. 1. Proposed integrated electricity-free radiative cooling, membrane adsorption, solar heating and desorption, and CO_2 product for further purification and utilization.

2.2.2 Develop Membrane Adsorbents

One of the key challenges for adsorption, heating, desorption, and cooling of the adsorbents is the long time needed for the mass transfer and heat transfer. Ideally, the adsorbents should be embedded in a macroscopic scaffold that effectively exposes them to the air and can be easily heated for desorption. We proposed a novel sorbent-containing highly porous, flat-sheet membrane platform (20-100 μm) to decrease the cycle time and thus increase the capacity of CO_2 adsorption. The porous membranes with a porosity of 60 – 95% can contain CO_2-philic polymers such as polyethylenimine (PEI). Similar to the hollow fiber membranes (HFM)-based adsorbents,[36-39] our membrane sorbents can be fabricated using existing membrane fabrication equipment and allow for similar CO_2 capture as packed bed systems while significantly reducing pressure drop and accelerate the adsorption and desorption. On the other hand, the flat-sheet platform allows easy packaging into systems with low pressure-drop, and the SINCs can be well-dispersed in these highly porous polymers to further reduce mass and heat transfer resistance compared with the MOFs used in the HFM adsorbents.

2.2.3. Design CO_2-philic SINCs

MOFs are a class of porous materials that have attracted much attention due to their permanent porosity and ability to be tuned at the molecular level through straightforward modular synthetic methods.[40] MOFs are formed by the assembly of metal-containing nodes (metal ions or metal-based clusters) that function as structural building units and organic ligands.[41] CO_2 capture is one of the most active and attractive research areas in MOF's applications.[42] The primary challenge of MOF sorbents is their slow adsorption/desorption rate and affinity for CO_2 such that they can capture at the relatively low concentrations found in air. To overcome these challenges, we proposed SINCs as an alternative sorbent, guided by recent successes in the MOF literature. There is a growing library of MOFs that are capable of direct air capture,[42] and the proposed SINC sorbent materials exploit all of their promising features (high selectivity, high uptake, long-term stability) while reducing adsorption and desorption times to a fraction of those required by frameworks. This reduction is made possible because (i) SINCs obviate the need for air/CO_2 to diffuse throughout large crystallites, and (ii) SINCs are <10 nm in diameter and can therefore be incorporated into ultra-thin films that enable innovations to air-capture design, as shown in Fig. 2.

Even when synthesized as a microcrystalline powders, MOFs range from 150-200 nm, orders of magnitude larger than SINCs. Furthermore, SINCs may be readily functionalized to either enhance mixing into polymers or for covalent incorporation into polySINCs, analogous to recently emerging polyMOFs. The use of ultrathin porous membranes (i.e. 20-100 μm thick) increases the mass transfer of air to the sorbent sites and decreases the pressure drop, leading to super-fast sorption and desorption and lower energy.

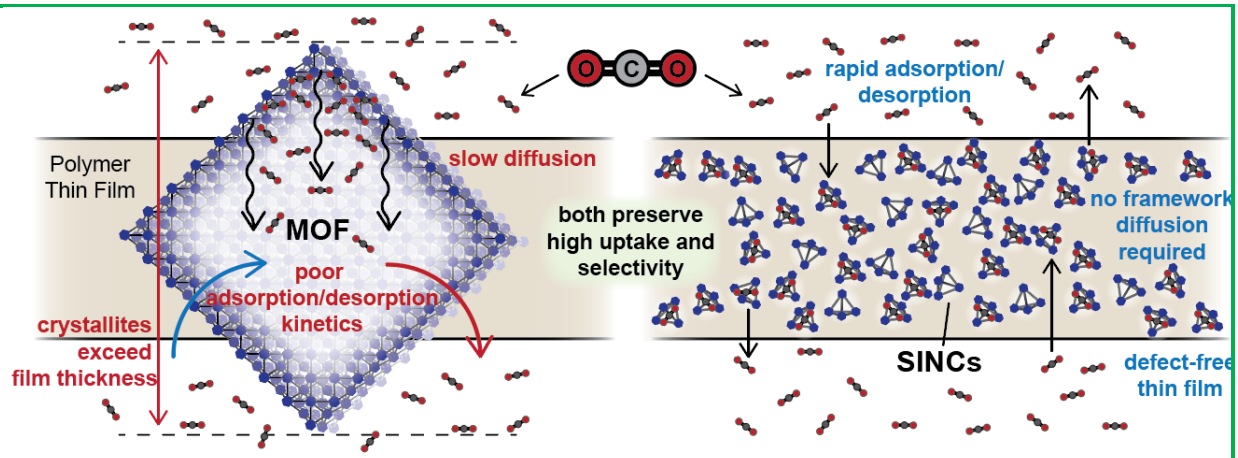

Fig. 2. SINC sorbents preserve the high uptake and selectivity of MOFs for DAC while improving upon processability and the kinetics of capture and release of CO_2

We identified Cu-based SINCs as sorbent materials stems from studies of the CO_2 uptake behavior of two frameworks and a cage. Like many other MOFs, Cu-based materials greatly benefit from the addition of amines. In particular, the addition of exogenous amines to Cu-BTTri, a Cu-MOF with a tris-triazolate bridging ligand (Fig. 3). At pressures higher than those relevant for DAC, but relatively low overall (up to 0.06 bar) Cu-BTTri with added ethylenediamine showed an uptake of 0.366 mmol/g versus 0.277 mmol/g when the base was absent.[43] Although measurements weren't made at lower pressures, it was noted that the enhancement from the added base was greater at lower pressures, suggesting that the effect may be even more relevant for DAC. The strategy of adding base has been proven at 400 ppm CO_2 for other MOFs. For example, a Mg-MOFs (MOF-74) shows an improvement from 0.14 mmol/g to 1.51 mmol/g upon the addition of ethylenediamine.[44] A related Mg-MOF improves from 0.13 mmol/g to 2.83 mmol/g when adding the same base.[45] Although these are not Cu-based materials, the principle is the same: the base binds to the open metal sites, and the CO_2 then interacts with the other N-atom site. We surmise that these order-of-magnitude improvements will translate to the Cu-SINCs since the same effect has been observed in Cu-MOFs.

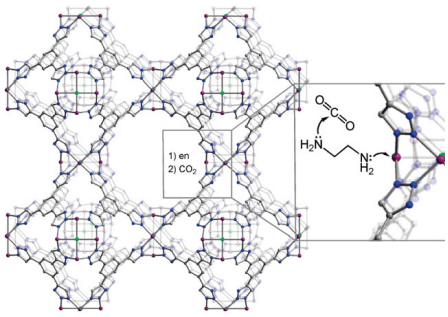

Fig. 3. Uptake capacities for DAC by Cu-MOFs may be enhanced by the addition of exogenous bases.

A second framework that motivates our sorbent design is HKUST-1, a well-known MOF that has been studied as a DAC sorbent for CO_2. Although we note that at low CO_2 pressures (0.04 mbar) the uptake capacity of HKUST-1 is not competitive with other MOF sorbents, with a value

of 0.05 mmol CO_2/g, the presence of open-metal sites at the Cu-paddlewheel nodes provides the basis for interactions with carbon dioxide.[46] Two Cu-paddlewheel motifs may be combined into the smallest possible SINC, containing only two nodes bridged by four ligands. The Cu-Cu separation in these so called Single Molecule Traps or SINCs is optimized for binding carbon dioxide. Despite the higher density compared to MOFs and relatively low number of metal nodes, this material has an uptake capacity of 0.63 mmol/g at 1 bar of CO_2.[47].

We hypothesized that Cu-SINCs may serve as high-uptake DAC sorbents by combining the design features of these three materials. We synthesized Cu-SINCs that increase the number of nodes from two to twelve to improve uptake capacity by introducing additional open metal sites. Lastly, because the internal cavity of the expanded Cu-SINCs is larger, it will be possible to add exogenous bases to exploit the DAC enhancements that similarly occur when adding nitrogenous bases to a number of MOFs with open metal sites.[13, 43]

2.2.4. Solar heating and electricity-free radiative cooling

While the solar heating has been widely practiced, daytime radiative cooling recently emerging as a promising technology to passively cool even under direct sunlight by combining a solar reflector with a thermal emitter.[48] The reflector functions in the visible to the near-infrared spectral region where solar energy is concentrated.[49-51] It functions as a good thermal emitter in the mid-infrared spectral region where room-temperature objects emit most of their radiation energy. Such spectral mismatch is achieved by using nanoscale optical engineering.[52-61]

In a prior project, co-PI Gan demonstrated electricity-free radiative cooling that operates under direct sunlight.[62] It does not use any energy and yet can provide a cooling power of ~ 100 W/m^2 through passive radiative cooling that reaches sub-ambient temperature. It consists of layers of polydimethylsiloxane (PDMS) on an aluminum (Al) substrate with a thickness of 100 μm and 1 mm, respectively. The thermal radiation is primarily emitted by the PDMS layer, which has a near-unity emissivity for wavelengths longer than 4.5 μm due to Si–O and Si–C bond vibrations (Fig. 4a), given sufficient film thickness (i.e. larger than 100 μm as modeled in Fig. 4b). Simultaneously, PDMS is transparent to sunlight, which is efficiently reflected by the Al substrate. The resulting emissivity is shown as the red line in Fig. 4a.

The emissivity of the structure is characterized using Fourier transform infrared (FTIR) spectroscopy. Our daytime radiative cooler system reflects almost 96% of the solar radiation (0.3~4 μm) and emits efficiently in the mid-IR region (>4 μm). We placed the radiator inside an insulating box made from polystyrene. A polyethylene film covers the opening of the box to reduce convective heat losses. In addition, we employed a selective solar absorber to develop a V-shaped beam-shaping structure to guide the thermal radiation (see the photo in the inset of Fig. 4c). Fig. 4d compares the temperature of the system (red curve) and the ambient air (grey curve) in 48 h. Our cooler achieves a temperature reduction of about 7 °C throughout the day, validating the electricity-free cooling under the sun.

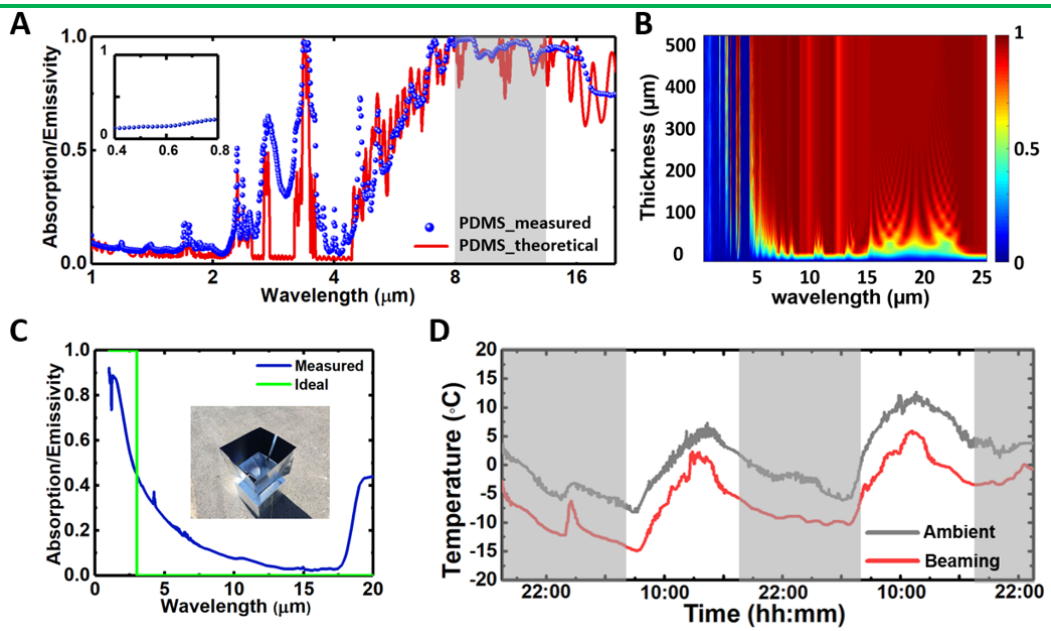

Fig. 4. (A) Absorption/emissivity spectra of a planar PDMS/aluminum film with a thickness of 150 μm (the solid curve shows numerical modeling, and the spheres represent measured data). The inset shows that the PDMS film also absorbs part of the solar irradiation in the visible and near-infrared regime. (B) The modeled absorption spectra of the planar PDMS/aluminum film as the function of the PDMS film thickness. (C) Absorption spectra of an ideal selective absorber (green line) and a commercial spectral selective absorber (blue line). (D) A continuous 48 h cooling test: the grey line indicates the ambient temperature, and the red line is the temperature in the beaming system.

3. Project Achievement

3.1. Project Management

Table 2 summarizes the milestones designed to evaluate the progress of the project. We had fully met the milestones and targets. The detailed technical achievements are shown below.

Table 2. Overview of project milestone status.

Milestone Title/Description	Completion Date	Verification Method
Project Management Plan	10/31/20	PMP file
Technology Maturation Plan	12/31/20; 12/31/22	TMP file
Project Kickoff Meeting	12/31/20	Presentation
Project Review Meeting	10/31/22	Presentation
Technology EH&S Risk Assessment	1/31/23	Report file
Demonstrate scalable synthesis (>5 g per batch) of porous polymers compatible with SINCs	3/31/21	Quarterly report
Demonstrate scalable synthesis (>5 g per batch) of SINCs with uptake capacities of >1 mmol CO_2/g sorbent	9/30/21	Quarterly report
Membrane adsorbents with CO_2 adsorption capability of 1.5 mmol/g	3/31/22	Quarterly report
A portable device constructed for DAC with a footprint of < 0.5 m^2 and weight of < 10 kg	6/30/22	Quarterly report
100-h continuous operation of the DAC with 5 g/h CO_2 captured	8/31/22	Quarterly report

Final techno-economic analysis	11/30/22	Reports

3.2. Synthesis and Characterization of SINCs

SINCs are an attractive alternative to metal-organic frameworks (MOFs) owing to their solubility, which enables solution-state processing, and their inherent pore structure. Current state-of-the-art DAC technologies rely upon various alkylamine solutions which capture CO_2 through the formation of carbamates; however, these are plagued by poor cyclability and require significant energy input to remove the captured CO_2. By incorporating alkyl amine functionalities in the SINC building blocks we aimed to form processible cages with permanent porosity which selectively capture CO_2 and can be interfaced with polymeric materials.

Initial SINC targets were Zr-based cages bearing primary alkyl amine functional groups and Cu paddlewheel-based cages with aryl amine bridging groups. The formation of Zr-based SINCs uses 1,4-benzenedicarboxylate building blocks, our strategy was to functionalized the structural building block with primary alkyl amine groups via ether linkages as illustrated in Scheme 1 from commercially available precursors. Briefly, the novel OPA and OPA-NH_2 ligands were synthesized via a Williamson ether synthesis using *N*-boc protected 3-bromopropylamine, followed by subsequent deprotection under acidic conditions.

Scheme 1. Synthesis of OPA and OPA-NH_2 building blocks for Zr-SINC construction.

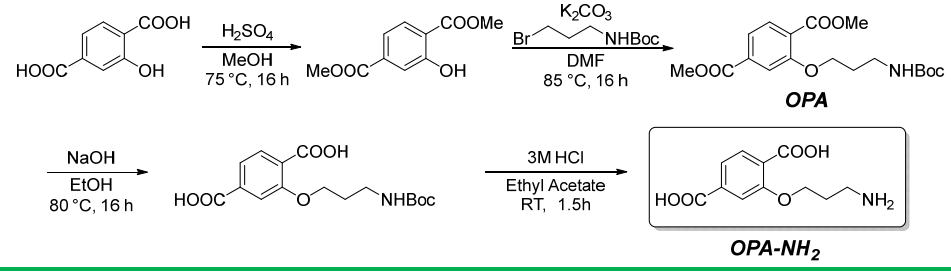

With amine-functionalized ligands in hand, self-assembly chemistry was subsequently explored. Self-assembly reactions were performed using zirconocene dichloride (Cp_2ZrCl_2) as the Zr-precursor which undergoes hydrolysis to form the structurally integral $Cp_3Zr_3(\mu^2\text{-}OH)_3(\mu^3\text{-}O)$ cluster (see Figure 5). Coordination of 180° dicarboxylate donors results in either the V_2L_3 "lantern" (as illustrated in Figure 5) or V_4L_6 tetrahedral SINCs depending on ligand dimension (where V represents a Zr-cluster vertex, and L is a functionalized dicarboxylate ligand). Changes in chemical shift in the ^1H NMR suggest that coordination of the OPA or OPA-NH_2 ligand occurs under reaction conditions. 2D DOSY spectra supports the formation of a single species in solution with resonances attributed to the Zr-cluster, and organic ligand possessing the same diffusion coefficient, see Figure 6. We have found that exchanging the outersphere chloride counterions for triflates leads to enhanced solubility, which ultimately leads to greater processability when incorporating the SINCs into a polymer matrix. Counterion exchange was performed by treating the SINC with AgOTF.

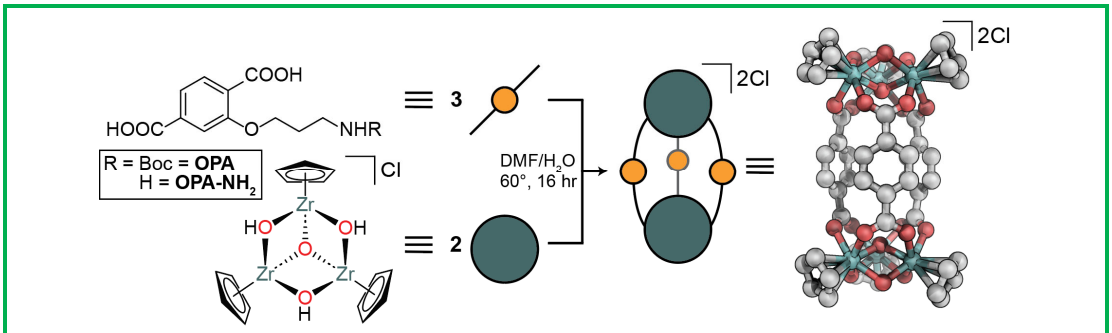

Figure 5. Illustration of the self-assembly reaction between $Cp_3Zr_3(\mu^2\text{-}OH)_3(\mu^3\text{-}O)$ cluster formed in situ and OPA or OPA-NH_2 ligand to form the V_2L_3 lantern assembly. Linker side chain R-groups have been omitted for clarity from the model.

Mass spectrometry was then used to assess the stoichiometry of the singular species in solution. High-resolution ESI-FT-ICR mass spectra were acquired for SINCs formed with OPA and OPA-NH_2 linkers. In both cases the SINC form was found to possess a V_2L_3 stoichiometry, indicative of a lantern topology. Figure 6 is a representative example of a mass spectrum of these SINCs, in this case, the triflate exchanged [Zr-OPA-NH_2]$(OTf)_2$ lantern. The base peak (m/z = 891.4196) corresponds to [Zr-OPA-NH_2]$^{2+}$, the intact SINC ionized by the loss of the outersphere OTf^- anions. The other major peaks could be assigned to various ionization modes of the intact SINC. Notably, we see no evidence for the formation of any V_4L_6 tetrahedral cages, this suggests that the Zr-OPA and Zr-OPA-NH_2 SINCs selectively form lantern structures with no equilibrium between the two topologies. This understanding is critical for developing structure-functional relationships.

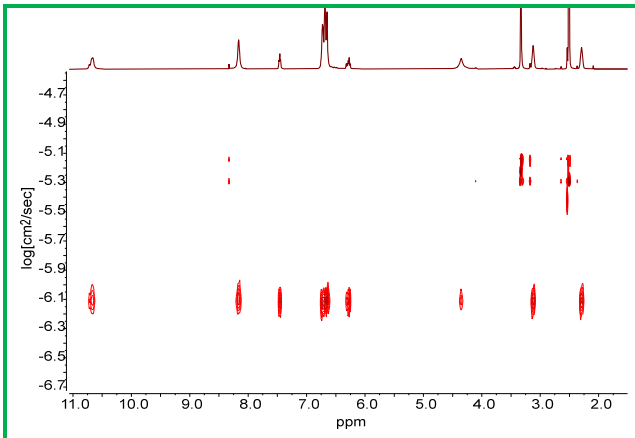

Fig. 6. [Zr-OPA-NH_2]Cl_2 cage DOSY NMR spectrum. Two distinct diffusion coefficients are observed attributed to residual solvent from synthesis, and the SINC.

The CO_2 capacities of the amine rich SINCs were examined. Three different amine-containing SINCs were tested: Zr-OPA, Zr-OPA-NH_2, and Zr-NH_2 which replaces the ether side chain with an anilinic nitrogen (see Table 3). There is little enhancement in CO_2 capacity using 400 ppm CO_2 when comparing aryl amine to the Boc protected amine. In both systems the nucleophilicity of the nitrogen lone pair is diminished by the aromatic system of the aryl amine and carbonyl group of the Boc protected amine. When the Boc group was removed leaving a primary alkyl amine there was a 130% increase in CO_2 capacity, reflecting the enhancement in nucleophilicity, and leading to greater -NH_2–CO_2 interactions. These results support our initial hypothesis that amine decorated SINCs are competent for DAC of CO_2.

In addition to the work decorating SINCs with primary amines, we have also developed synthetic routes to olefin functionalized cages. These linkers offer the opportunity to develop post-synthetic modification chemistry whereby amine moieties may be introduced after the formation of the SINC. Literature precedent exists for post-synthetic modification of analogous MOFs; however, this approach has remained largely unexplored in SINCs. Briefly, we hypothesize that a terminal olefin can be dihalogenated followed by treatment with ammonia to furnish veritable polyaminated SINCs. Notably, unlike the amine functionalized SINCs, self-assembly with the 2-allyl-1,4-benzendicarboxylate linker resulted in the tetrahedral cage rather than the lantern which was confirmed spectroscopically (see Figure 7). Work is ongoing to optimize post-synthetic halogenation and amination steps.

Table 3. CO_2 uptake measurements on amine-rich SINCs using 400 ppm CO_2 in N_2.

Sample	*CO_2 capacity (mmol CO_2/g sorbent)*	*Amine efficiency**
Zr-NH_2	0.13	7.3 %
Zr-OPA	0.10	7.2 %
Zr-OPA-NH_2	0.23	14.2 %

*Amine efficiency = (n_{CO2}/n_N)•100

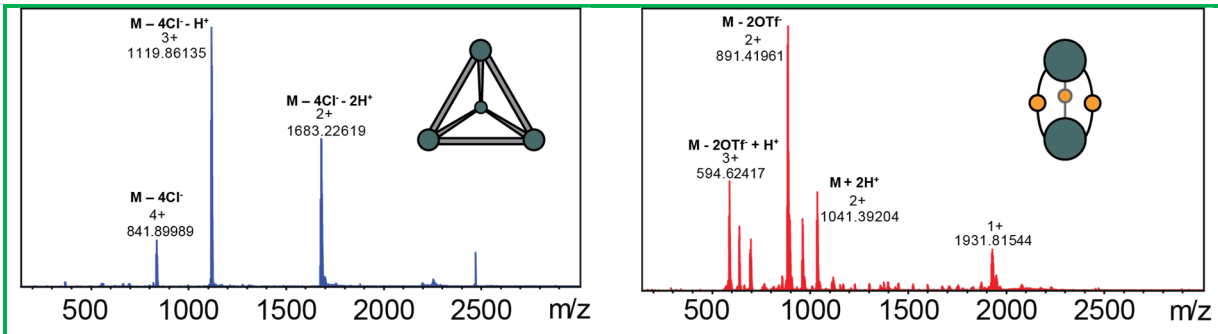

Fig. 7. (Top, red) High resolution ESI-FT-ICR mass spectrum of Zr-OPA-NH_2 where M = [Zr-OPA-NH_2](OTf)$_2$ lantern SINC. (Bottom, blue) High resolution ESI-FT-ICR mass spectrum of Zr-allyl where M = [Zr-allyl](OTf)$_4$ tetrahedral SINC.

MOP-15 is a known amine-functionalized cuboctahedral copper cage with a $M_{24}L_{24}$ architecture synthesized via self-assembly. The structural metal nodes are 12 dinuclear copper paddlewheels linked by 12 5-amino-1,3-benzenedicarboxylate ligands. After synthesis, we activate the bulk material under dynamic vacuum. Activations acts to remove Cu-coordinated and pore space adsorbed solvent molecules resulting in open coordination site Cu-centers which can be leveraged to enhance noncovalent CO_2-cage interactions. Comparing the infrared spectra of the starting materials to the spectrum of the resulting Cu-based SINC supports formation owing to features of both components present in the final material (see Figure 8).

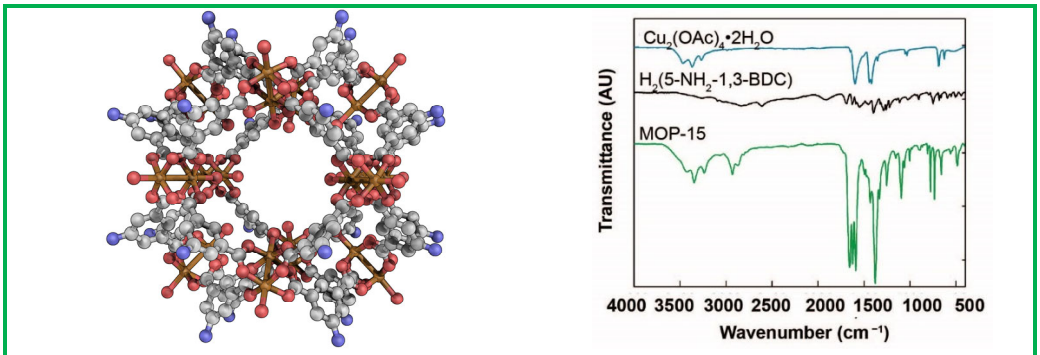

Fig. 8. (Left) Crystal structure of MOP-15 from literature (Cu = orange, N = blue, O = red, C = gray). (Right) IR spectra of starting materials $Cu_2(OAc)_4•2H_2O$ (blue) and 5-amino-1,3-benzenedicarboxylate (black) and MOP-15 (green).

3.3. Prepare and Characterize Membrane Adsorbents

We have prepared porous membranes based on commercial Solupor support with a pore size of 0.9 µm and porosity of 86%. The Solupor was infiltrated with various PEI loadings via wet-impregnation. Two different molecular weights PEI were investigated, i.e., Mn = 800 g/mol (PEI800) and 25,000 g/mol (PEI25k). The PEI content of 14-48 wt.% in the was achieved while retaining high porosity (above 70%), indicating that part of the PEI is dissolved in the polymer phase, instead of the pores. Higher PEI molecular weight seems to increase the loading while retaining higher porosity (as shown in Table 4). The PEI infiltration does not significantly decrease the gas permeance or increase gasflow resistance.

Table 4. Effect of impregnation of PEI in the Soloupor membranes on the porosity and gas transport resistance.

Coating solutions	PEI content in membranes (wt%)	Porosity (%)	Gas permeance (GPU)	
			CH_4	CO_2
None	0	86	34,000	23,000
1% PEI800	14	82	110,000	62,000
3% PEI800	36	73	94,000	58,000
5% PEI800	44	70	34,000	23,000
1% PEI25K	16	85	113,000	65,000
3% PEI25K	35	79	76,000	48,000
5% PEI25K	48	75	33,000	22,000

We determined the CO_2 adsorption capacity of the membrane adsorbents via a thermal gravimetric analyzer. Three adsorbents containing varied PEI800 contents were prepared to investigate the effect of adsorbent composition on CO_2 capture capacity. Table 5 shows the effect of PEI800 content in SINCs/PEI adsorbent on CO_2 capture capacity @ 400ppm CO_2 and 35ºC. As the PEI800 content increases from 5 to 67 wt.%, the CO_2 capture capacity decreases significantly from 0.08 to 0.02 mmol/g. Interestingly, the sample containing 5 wt.% PEI800 shows the CO_2 capture capacity slightly lower than the SINCs (i.e., SINCs-0), presumably because the PEI blocks the accessible cavities of SINCs for CO_2 adsorption.

Table 5. CO_2 capture capacity of the membrane adsorbents comprising SINCs and PEI800 when tested with the air containing 400 ppm CO_2 at 35ºC.

Samples	PEI800 content (wt%)	CO_2 capacity (mmol CO_2/g)
SINCs-0	0	0.10
SINCs/PEI-1	5	0.08
SINCs/PEI-2	33	0.06
SINCs/PEI-3	67	0.02

Table 6 compares the CO_2 capture capacity of membrane adsorbents with or without SINCs with 400 ppm CO_2 at 22ºC. With the incorporation of 2.2 wt.% SINCs, the CO_2 capacity increases by 16% from 0.50 mmol/g to 0.58 mmol/g.

Table 6. Comparison of CO_2 sorption capacity between membrane adsorbents with and without SINCs (i.e., NH_2-cage) for the air containing 400 ppm CO_2 at 22 ℃.

Samples	SINC content (wt%)	CO_2 sorption capacity (mmol CO_2/g)
PEI800-44	0	0.50
PEI800-44/NH_2-cage	2.2	0.58

Figure 9 shows that further increase of the PEI content to 64 mass% does not increase the CO_2 sorption and decreases the amine efficiency when tested with the air containing 400 ppm CO_2 and 25°C, which can be ascribed to the slow diffusion of CO_2 into the bulk PEI film. Specifically, when PEI content increases from 44 mass% to 64 mass%, the CO_2 capacity slightly decreases from 0.50 to 0.46 mmol/g, and the amine efficiency decreases significantly from 0.07 to 0.04 mol CO_2/mol N.

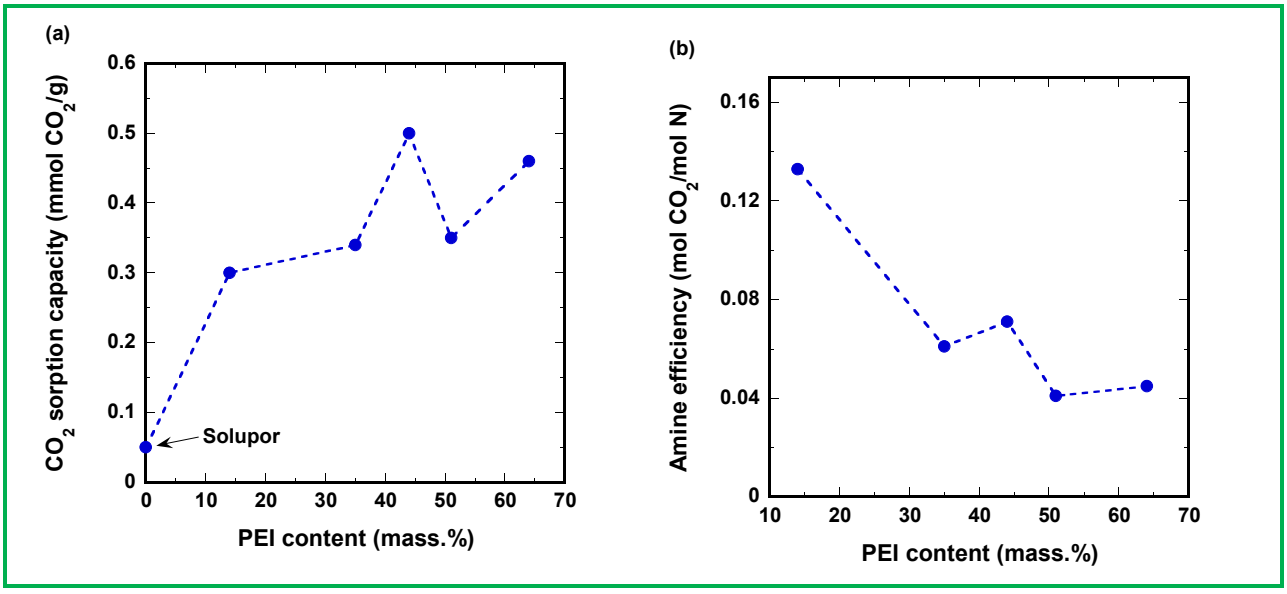

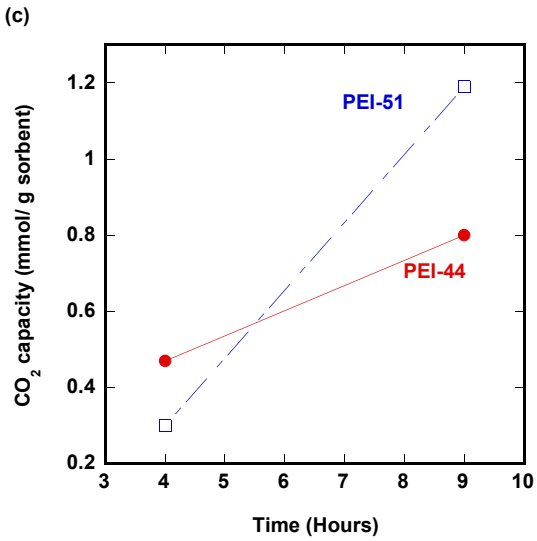

Fig. 9. Effect of PEI800 content on (a) CO_2 sorption capacity and (b) amine efficiency. (c) Effect of sorption time on CO_2 capacity for PEI-44 and PEI-51.

Figure 9c shows that increasing the temperature from 25 to 50°C doubles the CO_2 sorption from 0.45 to 0.90 mmol/g for PEI-44. A similar behavior was observed for PEI-51. For the highest PEI content sample, PEI-64, the effect of temperature on CO_2 capacity is less significant. Additionally, increasing the adsorption time from 4 to 9 h almost doubles the CO_2 sorption from 0.45 to 0.81 mmol/g in PEI-44 and from 0.35 to 1.2 mmol/g in PEI-51, indicating that the diffusion can be rate-limiting during the sorption.

Figure 10a illustrates the effect of relative humidity (%RH), ZrOPA loading, and temperature on CO_2 sorption capacity (mmol/g PEI). Increasing the %RH from 0% (dry condition) to 30%RH doubles the CO_2 sorption for all samples with and without ZrOPA. PEI/ZrOPA-5 exhibits the highest sorption capacity of 3.2 mmol/g at 30%RH and 25°C. However, the effect of %RH on CO_2 capacity at 35°C is less noticeable than that at 25°C

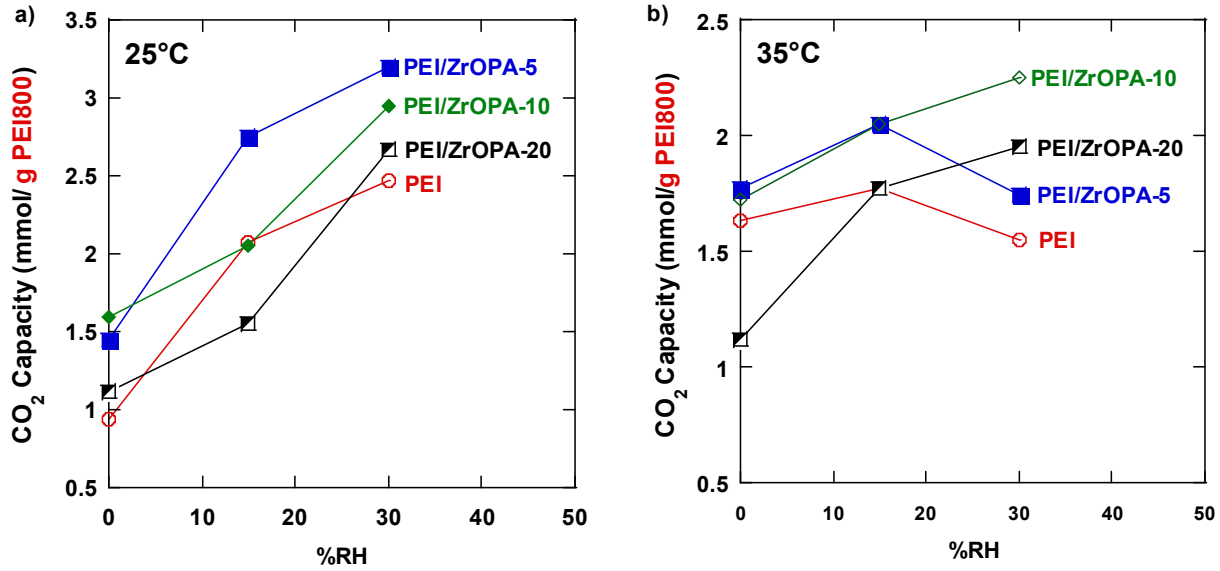

Fig. 10. Effect of %RH on CO_2 sorption capacity in the PEI/ZrOPA at (a) 25°C and (b) 35°C

Figure 11 displays 4 adsorption/desorption cycles in PEI-44. The CO_2 sorption capacity decreases by 23% from 0.31 mmol/g (1st cycle) to 0.24 mmol/g (4th cycle).

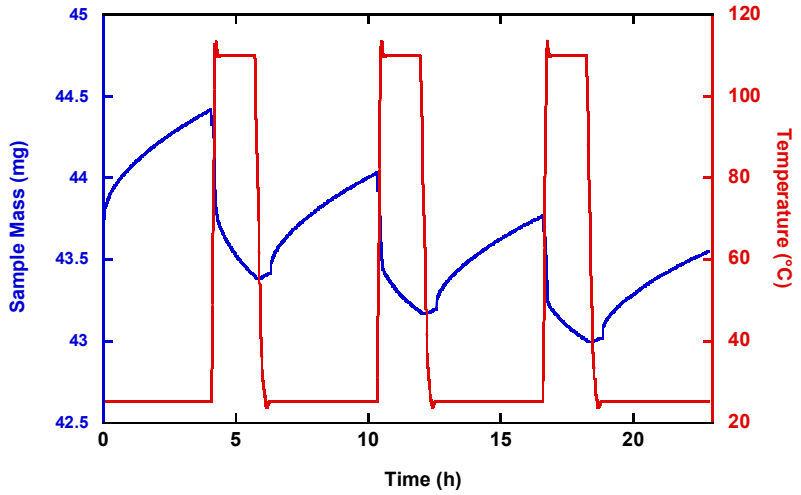

Cycle#	CO_2 capacity (mmol CO_2/g sorbent)
1	0.31
2	0.28
3	0.26
4	0.24

Fig. 11. Adsorption/desorption cycles of PEI-44. Adsorption: 400 ppm CO_2 in air at 25°C. Desorption: 110°C in N_2.

We performed 6 cycles of adsorption/desorption with a total of 50-h continuous operations, and the results are summarized in Figure 12. The adsorption was at 25°C using dry air containing 400 ppm CO_2, and the desorption was at 110°C under N_2 atmosphere. There was a decrease in the sample mass and CO_2 uptake (mg) in the first 4 cycles. After that, the CO_2 sorption capacity levels off at 0.37 mmol/g.

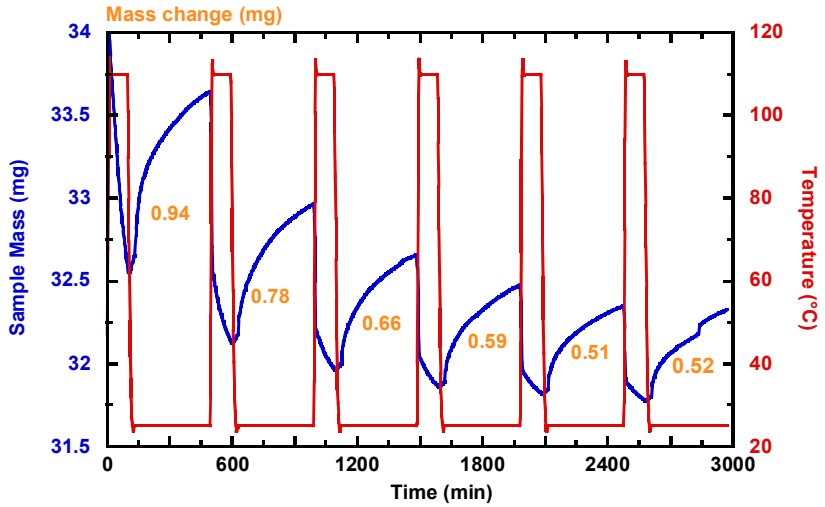

Cycle #	CO_2 sorption capacity (mmol CO_2/g)
1	0.66
2	0.55
3	0.47
4	0.42
5	0.37
6	0.37

Fig. 12. Adsorption/desorption cycles of PEI-44. Adsorption: 400 ppm CO_2 in the air at 25°C. Desorption: 110°C in N_2.

We performed 18 rapid cycles of adsorption/desorption with a total of 54-h continuous operations in PEI-48, as summarized in Figure 13. The adsorption was at 25°C using dry air containing 400 ppm CO_2 for 2 h, and the desorption was at 110°C under N_2 atmosphere for 15 min. The average working capacity of the adsorbent at these conditions is 0.12 mmol/g.

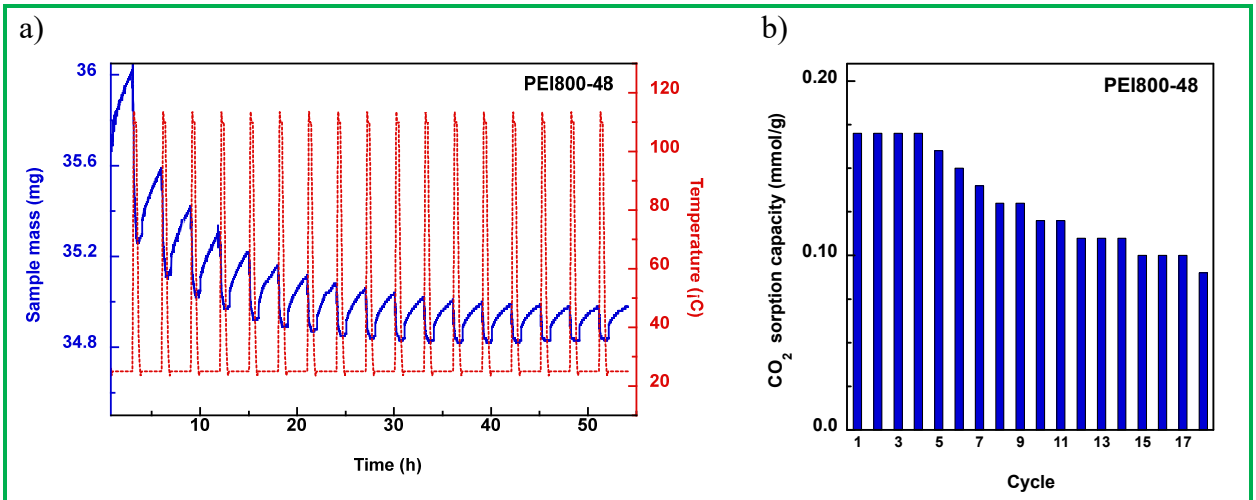

Fig. 13. (a) Sample mass and temperature profile for 18 cycles of adsorption/desorption with the air containing 400 ppm and (b) the CO_2 sorption capacity of each cycle.

3.4. Design New Materials for Radiative Cooling

We prepared radiative cooling emitters using PDMS for daytime radiative cooling. To minimize the solar absorption of the emitter and substrate, we fabricated two porous PDMS foams with different pore structures (porous PDMS_1 and porous PDMS_2) and compared them with a bare PDMS. We first characterized the micromorphology of these PDMS emitters. As shown by the SEM images in Fig. 14, the pore size of the porous PDMS_1 is around 300 µm, whereas the pore size of the porous PDMS_2 is mainly distributed from 300 µm to 20 µm. These smaller pores in porous PDMS_2 will slightly improve the optical scattering feature, as shown in Fig. 15.

Fig. 14. SEM images of porous PDMS_1, porous PDMS_2, and bare PDMS. The scale bar in the figure is 300 µm.

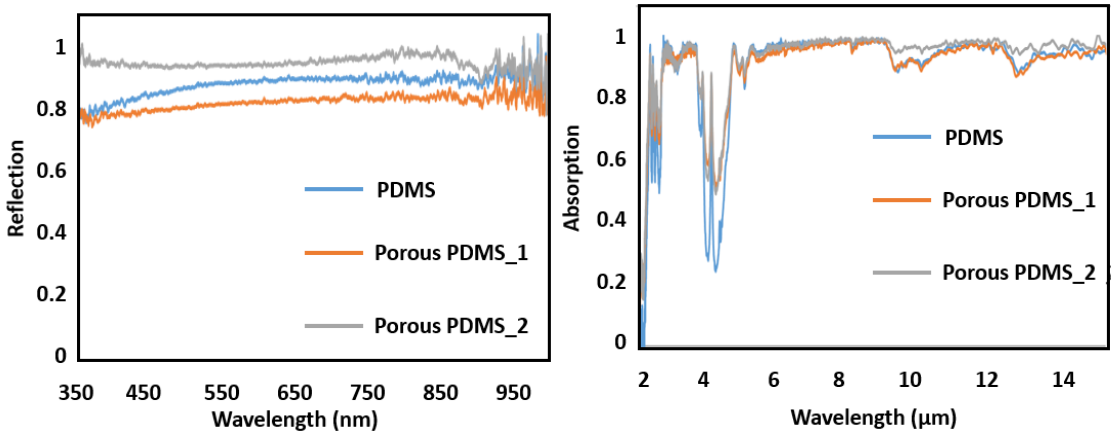

Fig. 15. The measured spectra of PDMS, porous PDMS_1, and porous PDMS_2 in the visible range (left) and mid-infrared range (right).

The measured absorption spectra indicate that the porous PDMS_2 (grey curve) shows the highest reflection (~97%) in the visible (VIS) range, which will significantly suppress the solar heating effect. On the other hand, all three PDMS emitters have over 95% absorption in the mid-infrared range. Particularly, as shown by the grey curve in the figure, the porous PDMS_2 shows slightly higher absorption/emission between 9 to 14 μm, which will further promote the radiative cooling performance.

Furthermore, we optimized the structure by embedding different nanoparticles into PDMS. In this reporting period, we mixed titanium dioxide (TiO_2) nanoparticles and aluminum particles with porous PDMS structures, respectively. The reflection spectra of obtained samples were characterized, as shown in Fig. 16. For aluminum embedded porous PDMS (blue curve), although aluminum particles can slightly enhance the reflection in the UV range (~96%), it will also enhance the absorption in the visible range (~76%), which will introduce strong solar heating effect. Meanwhile, the TiO_2 embedded porous PDMS (red curve) shows improved reflection in both VIS range (90%) and NIR range (97%), which is desired for daytime radiative cooling.

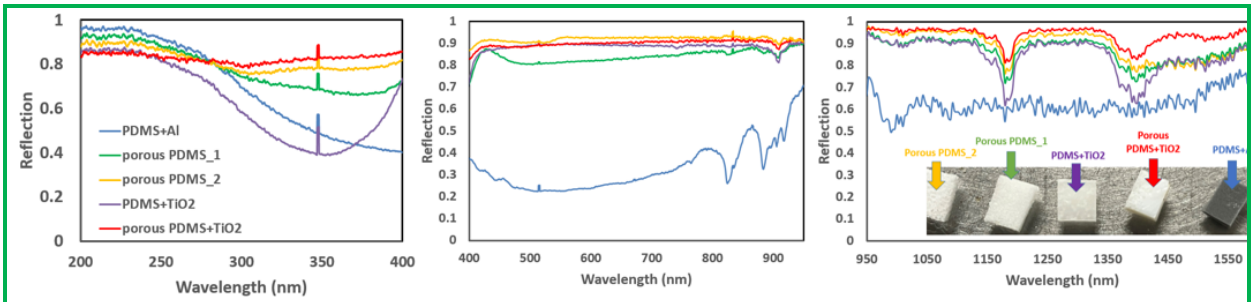

Fig. 16. Measured spectrum of different PDMS emitters in ultraviolet (UV), VIS and near-infrared (NIR) range.

The porous PDMS emitter for daytime radiative cooling was optimized for enhancing the solar reflection. Based on the porous structure reported in the last quarter, TiO_2 particles were embedded with PDMS at a weight ratio of 1%, 2%, 3%, and 5%, respectively. We characterized the VIS-NIR reflection spectra of the obtained samples and compared them to a non-embedded porous PDMS. As shown in Figure 17, all TiO_2 embedded porous PDMS show higher reflection than a non-embedded porous PDMS in VIS range (380-750 nm). In particular, a porous PDMS

embedded with 3%wt TiO_2 exhibits an average reflection of 96% from 380 nm to 750 nm and 90% from 750 nm to 1600 nm, which is desired for daytime radiative cooling.

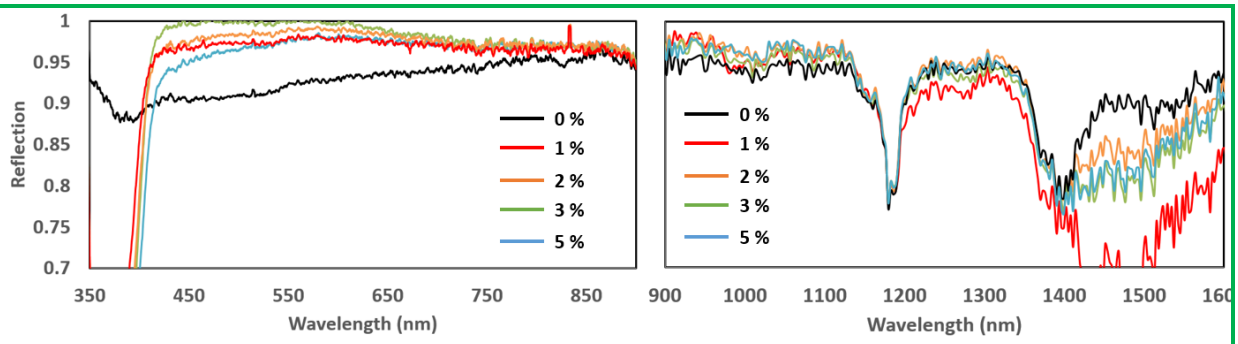

Fig. 17. The measured reflection spectra of the TiO_2 embedded porous PDMS in VIS-NIR range. The legend shown in the figures represent the weight ratio of the embedded TiO_2 particles.

We also investigated the surface morphology of obtained porous PDMS, as shown in Figure 18. The mean pore size of porous PDMS is ~200 μm, and the mean particle size of TiO_2 is ~300 nm. This hierarchical porous structure will induce a strong solar scattering effect, which explains the higher reflection of particle embedded porous PDMS. However, we also noticed that the particles formed aggravated clusters rather than dispersed particles, which may inhibit the solar scattering. Therefore, we will test different fabrication methods next.

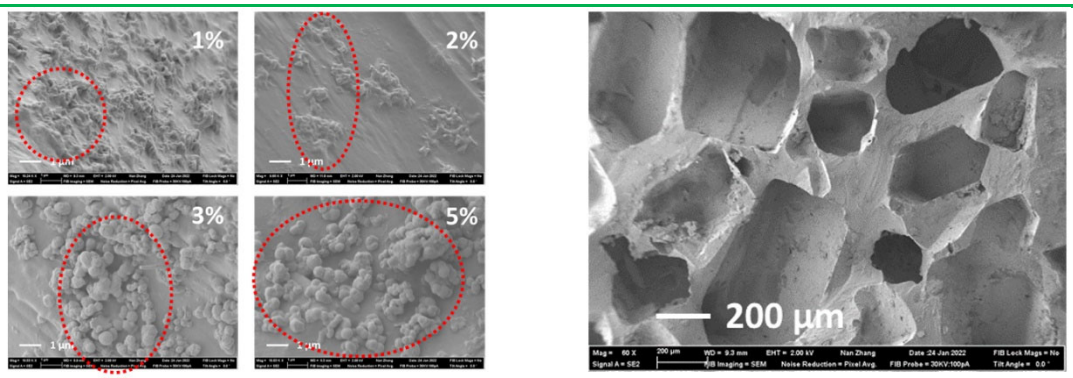

Fig. 18. The SEM images of TiO_2 embedded porous PDMS. The scale bar is 1 μm in the left figures and 200 μm in the right figure.

To obtain uniform distribution, two methods, i.e., magnetic stirring and ultrasonic, were employed when mixing the PDMS precursor with TiO_2 particles. The SEM images of the obtained samples shown in Figure 19 indicated that the ultrasonic process resulted in a more uniform particle distribution compared to the magnetic stirring process. The measured reflection spectra, as shown in Figure 20, also revealed that this uniform particle distribution led to a higher VIS reflection of 1.8%.

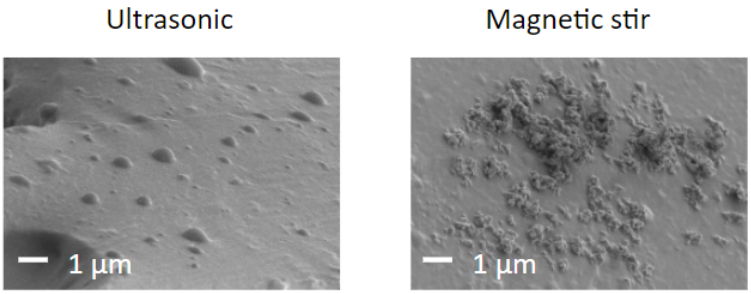

Fig. 19. The SEM images of TiO_2 embedded porous PDMS fabricated by ultrasonic and magnetic stirring. The scale bars are 1 µm.

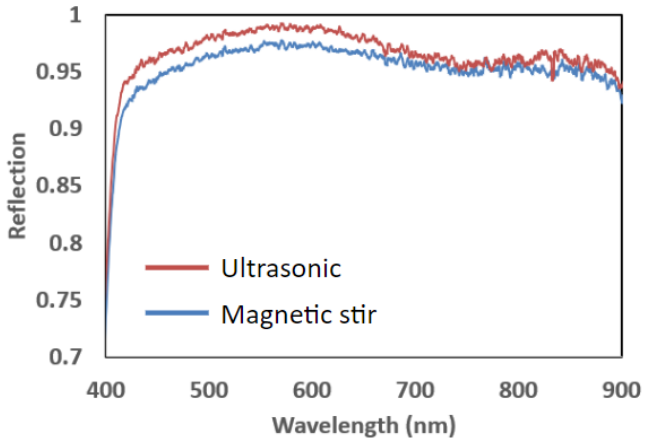

Fig. 20. The measured reflection spectra of the TiO_2 embedded porous PDMS fabricated by ultrasonic and magnetic stirring, respectively.

3.5. Lab-scale Demonstration of Continuous DAC

A prototype was constructed including radiative cooling chamber, water pump, solar heating chamber, and sorption/desorption chamber, as shown in Figure 21. We tested outside during the daytime to validate all the mechanical parts of the system, i.e., the rotating drum and cooling water pump.

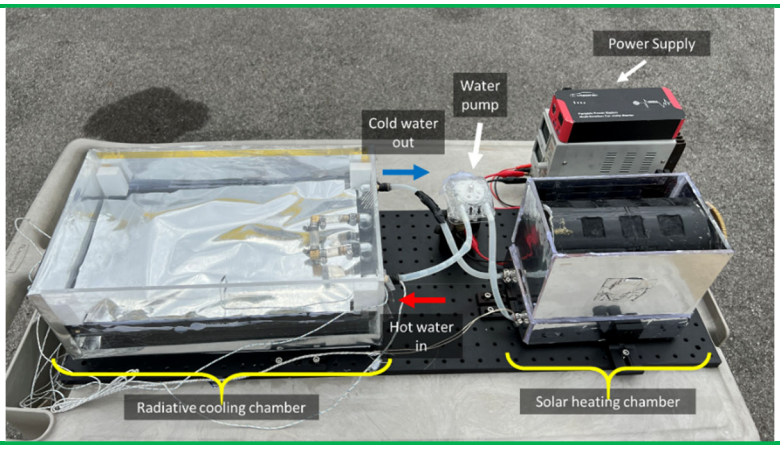

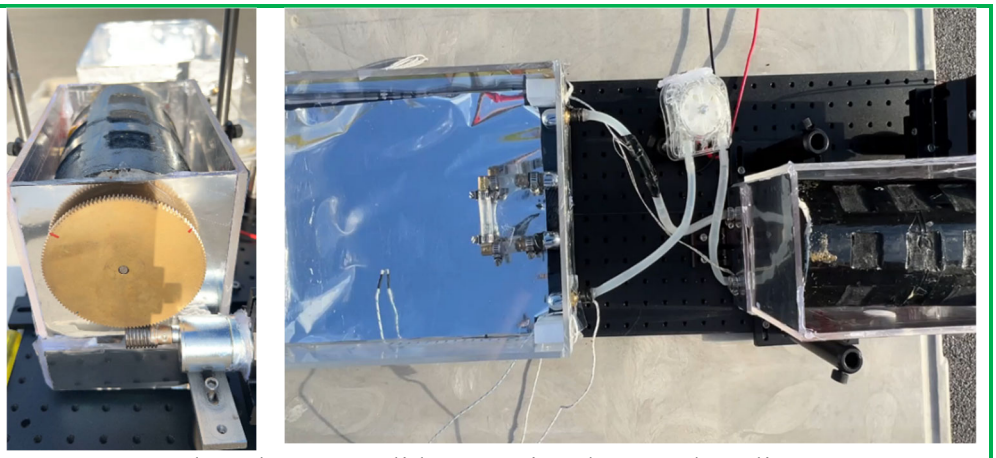

Fig. 21. Prototype tested outdoors to validate rotating drum and cooling water pump.

We further simplified the system for in-door operation. The fan, vacuum pump, heater, and CO_2 analyzer were fully integrated into the apparatus (Figure 22). The prototype was operated continuously for 100-h. However, the CO_2 concentration in the desorption stream was low due to the air leaking from the adsorption chamber when the vacuum was applied (Figure 23), resulting in a CO_2 capture rate below the 5 g CO_2/h captured target.

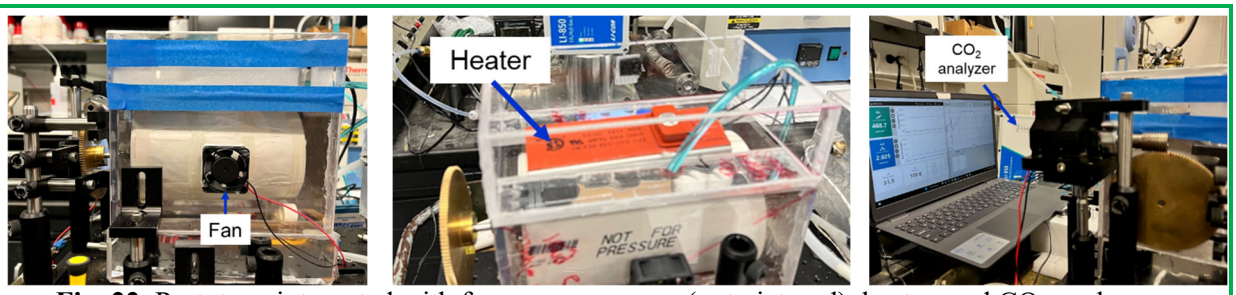

Fig. 22. Prototype integrated with fan, vacuum pump (not pictured), heater, and CO_2 analyzer.

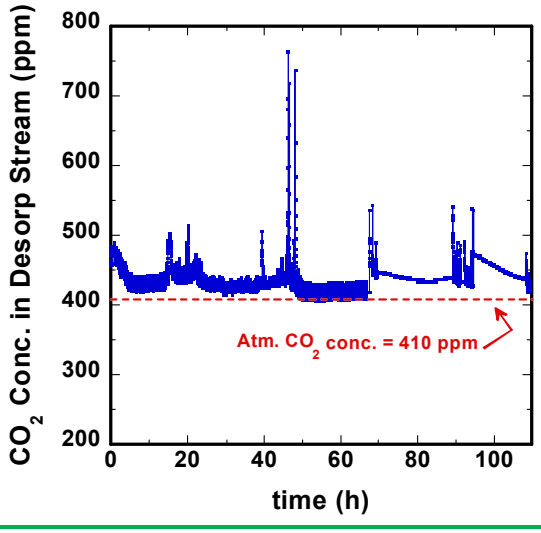

Fig. 23. CO_2 concentration in the desorption stream. The operating conditions include a vacuum rate of 10.1 L/h, an adsorbent mass of 0.840 g, a total CO_2 volume of 0.030 L, and total CO_2 sorption of 1.2 mmol CO_2.

3.6. Conceptual Process Design and TEA

Trimeric has prepared this conceptual technical and economic analysis of the University at Buffalo's membrane-based adsorbent process for direct air capture (as shown in Appendix I: State-Point Data). The process is currently at an early stage of development, and process inputs are limited. In order to estimate costs for UB's novel DAC process, Trimeric conducted an initial analysis based on a hypothetical implementation, which is relatively similar to more established solid-sorbent DAC processes. An example of the established process configuration is shown in Figure 24.

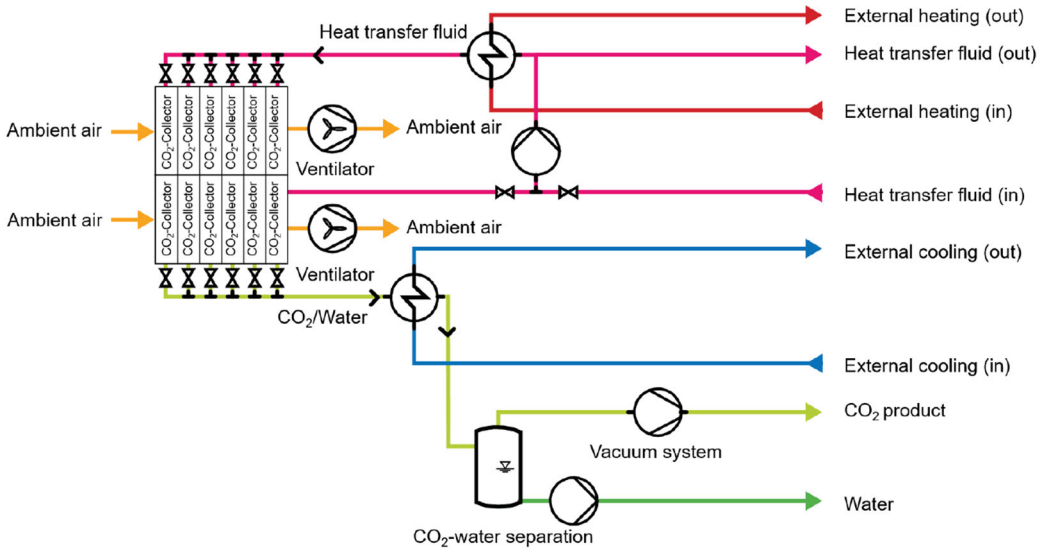

Fig. 24. Typical Sorbent-Based DAC System.

Trimeric's analysis reveals that in its current state, the process requires a high cost of capture ($1,343/tonne CO_2) with a total OPEX cost of $1,112/tonne CO_2. The adsorbent replacement cost accounted for 52% of the total OPEX cost.

Several sensitivity studies were conducted to assess and identify aspects of the process that make the most significant contribution to the overall cost of capture. The base case appears as the highest cost point on the graph at $10/kg adsorbent cost and adsorbent working capacity of 0.32 mol CO_2/kg adsorbent. Adsorbent cost is shown to be the stronger influence. As shown in Figure 25, with all other inputs unchanged, the adsorbent cost must be reduced to less than $2/kg for the total cost of capture to approach benchmark values. Additionally, increasing the service life above its current value of 0.5 years has the potential to significantly reduce the cost of capture. Holding everything else constant, there are diminishing returns when increasing the service life above 1 year.

a)

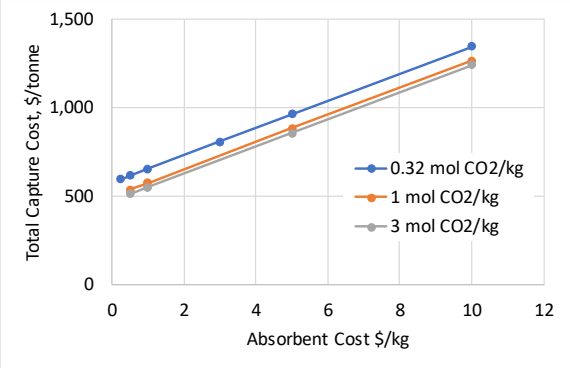

b)

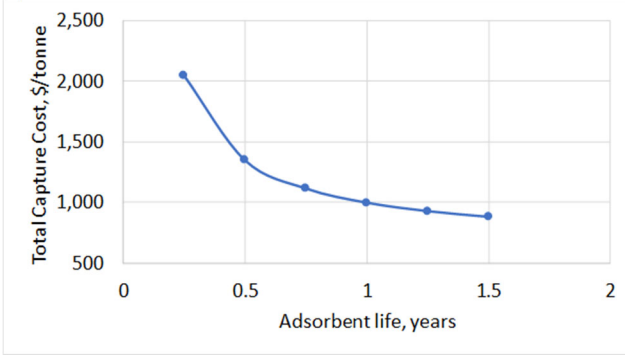

Fig. 25. CO_2 concentration in the desorption stream and a table summarizing the prototype operating conditions.

4. Products and Impacts

During this project, one Ph.D. student and one MS student received the inter-disciplinary training and graduated, including Dr. Lyu Zhou and Ms. Krysta Clark. Three postdoctoral researchers (Dr. Thien Tran, Matthew Crawley, and Amanda Grass) and four Ph.D. students (Vinh Bui, Jacob Rada, Heshali Welgama, and Dylan Tua) are involved in this project. The project leads to one peer-reviewed publication, one manuscript in preparation, and five oral presentations. The details are shown below.

1. L. Zhou, J. Rada, H. Zhang, H. Song, S. Mirniaharikandi, B. Ooi, Q. Gan, Sustainable and Inexpensive Polydimethylsiloxane Sponges for Daytime Radiative Cooling, Adv. Sci., 8 (23) 2102502, 10.1002/advs.202102502
2. H. Lin, T. R. Cook, Q. Gan, A. Sexton; Membrane Adsorbents Comprising Self-Assembled Inorganic Nanocages (SINCs) for Super-fast Direct Air Capture Enabled by Passive Cooling, Kickoff meeting with the DOE NETL team, November 10, 2020.
3. H. Lin, T. R. Cook, Q. Gan, A. Sexton; Membrane Adsorbents Comprising Self-Assembled Inorganic Nanocages (SINCs) for Super-fast Direct Air Capture Enabled by Passive Cooling, DOE NETL Project Review Meeting, February 24, 2021.
4. T. Tran, H. Lin, T. R. Cook, Q. Gan, A. Sexton; Membrane Adsorbents Comprising Self-Assembled Inorganic Nanocages (SINCs) for Super-fast Direct Air Capture Enabled by Passive Cooling, Carbon Management and Natural Gas & Oil Research Project Review Meeting, August 2021.
5. T. Tran, A. Chakraborty, S. Singh, A. Grass, T. R. Cook, and H. Lin, Membrane Adsorbents Comprising Self-Assembled Inorganic Nanocages (SINCs) for Direct Air Capture, AIChE 2021 Annual Meeting – Boston, MA, November 10, 2021.
6. Tran, T., "Membrane Adsorbents Comprising Self-Assembled Inorganic Nanocages (SINCs) For Direct Air Capture." American Institute of Chemical Engineer (AIChE) Conference, Phoenix, AZ, 11/22/2022

References:

(1) Lackner, K. S.; Ziock, H.-J.; Grimes, P. *Carbon dioxide extraction from air: Is it an option? Technical Report LA-UR-99-583 (Los Alamos National Laboratory)*; 1999.

(2) Keith, D. W., Why capture CO_2 from the atmosphere?, *Science* **2009,** *325* (5948), 1654-1655.

(3) Lackner, K. S.; Brennan, S.; Matter, J. M.; Park, A. H. A.; Wright, A.; van der Zwaan, B., The urgency of the development of CO_2 capture from ambient air, *PNAS* **2012,** *109* (33), 13156-13162.
(4) Keith, D. W.; Holmes, G.; Angelo, D. S.; Heidel, K., A process for capturing CO_2 from the atmosphere, *Joule* **2018,** *2* (8), 1573-1594.
(5) Davis, S. J.; Lewis, N. S.; Shaner, M.; Aggarwal, S.; Arent, D.; Azevedo, I. L.; Benson, S. M.; Bradley, T.; Brouwer, J.; Chiang, Y. M.; Clack, C. T. M.; Cohen, A.; Doig, S.; Edmonds, J.; Fennell, P.; Field, C. B.; Hannegan, B.; Hodge, B. M.; Hoffert, M. I.; Ingersoll, E.; Jaramillo, P.; Lackner, K. S.; Mach, K. J.; Mastrandrea, M.; Ogden, J.; Peterson, P. F.; Sanchez, D. L.; Sperling, D.; Stagner, J.; Trancik, J. E.; Yang, C. J.; Caldeira, K., Net-zero emissions energy systems, *Science* **2018,** *360* (6396), eaas9793.
(6) Azarabadi, H.; Lackner, K. S., Postcombustion capture or direct air capture in decarbonizing us natural gas power?, *Environ. Sci. Techn.* **2020,** *54* (8), 5102-5111.
(7) https://www.usea.org/event/workshop-direct-air-capture-technology-needs, Workshop on Direct Air Capture Technology Needs, Department of Energy and United States Energy Association. (accessed 5/24/2020).
(8) *National Academies of Sciences, Engineering, and Medicine. Negative Emissions Technologies and Reliable Sequestration: A Research Agenda*. The National Academies Press: Washington, DC, 2019.
(9) Goeppert, A.; Czaun, M.; Prakash, G. K. S.; Olah, G. A., Air as the renewable carbon source of the future: an overview of CO_2 capture from the atmosphere, *Energy Environ. Sci.* **2012,** *5* (7), 7833-7853.
(10) House, K. Z.; Baclig, A. C.; Ranjan, M.; van Nierop, E. A.; Wilcox, J.; Herzog, H. J., Economic and energetic analysis of capturing CO_2 from ambient air, *PNAS* **2011,** *108* (51), 20428-20433.
(11) Azarabadi, H.; Lackner, K. S., A sorbent-focused techno-economic analysis of direct air capture, *Appl. Energy* **2019,** *250*, 959-975.
(12) Shi, X.; Xiao, H.; Azarabadi, H.; Song, J.; Wu, X.; Chen, X.; Lackner, K. S., Sorbents for the direct capture of CO_2 from ambient air, *Angew. Chem. Int. Ed.* **2020,** *59* (18), 6984-7006.
(13) Sanz-Perez, E. S.; Murdock, C. R.; Didas, S. A.; Jones, C. W., Direct capture of CO_2 from ambient air, *Chem. Rev.* **2016,** *116* (19), 11840-11876.
(14) Tong, Z.; Ho, W. S. W., New sterically hindered polyvinylamine membranes for CO_2 separation and capture, *J. Membr. Sci.* **2017,** *543*, 202-211.
(15) Zhu, L.; Tian, D.; Shin, D.; Jia, W.; Bae, C.; Lin, H., Effects of tertiary amines and quaternary ammonium halides in polysulfone on membrane gas separation properties, *J. Polym. Sci. Part B: Polym. Phys.* **2018,** *56* (18), 1239-1250.
(16) Varghese, A. M.; Karanikolos, G. N., CO_2 capture adsorbents functionalized by amine-bearing polymers: A review, *Int. J. Greenh. Gas Con.* **2020,** *96*.
(17) Holewinski, A.; Sakwa-Novak, M. A.; Jones, C. W., Linking CO_2 sorption performance to polymer morphology in aminopolymer/silica composites through neutron scattering, *J. Am. Chem. Soc.* **2015,** *137* (36), 11749-11759.
(18) Ma, X.; Wang, X.; Song, C., "Molecular Basket" sorbents for separation of CO_2 and H_2S from various gas streams, *J. Am. Chem. Soc.* **2009,** *131*, 5777-5783.

(19) Wang, D.; Sentorun-Shalaby, C.; Ma, X.; Song, C., High-capacity and low-cost carbon-based "Molecular Basket" sorbent for CO_2 capture from flue gas, *Energy Fuels* **2011,** *25*, 456-458.
(20) Goeppert, A.; Meth, S.; Prakash, G. K. S.; Olah, G. A., Nanostructured silica as a support for regenerable high-capacity organoamine-based CO_2 sorbents, *Energy Environ. Sci.* **2010,** *3* (12), 1949-1960.
(21) Tanthana, J.; Chuang, S. S. C., In situ infrared study of the role of PEG in stabilizing silica-supported amines for CO_2 capture, *Chemsuschem* **2010,** *3* (8), 957-964.
(22) Sakwa-Novak, M. A.; Tan, S.; Jones, C. W., Role of additives in composite PEI/oxide CO_2 adsorbents: enhancement in the amine efficiency of supported PEI by PEG in CO_2 capture from simulated ambient air, *ACS Appl. Mater. Interfaces* **2015,** *7* (44), 24748-24759.
(23) Wurzbacher, J. A.; Gebald, C.; Steinfeld, A., Separation of CO_2 from air by temperature-vacuum swing adsorption using diamine-functionalized silica gel, *Energy Environ. Sci.* **2011,** *4* (9), 3584-3592.
(24) Drese, J. H.; Choi, S.; Lively, R. P.; Koros, W. J.; Fauth, D. J.; Gray, M. L.; Jones, C. W., Synthesis-Structure-property relationships for hyperbranched aminosilica CO_2 adsorbents, *Adv. Funct. Mater.* **2009,** *19* (23), 3821-3832.
(25) Yoo, S.; Lunn, J. D.; Gonzalez, S.; Ristich, J. A.; Simanek, E. E.; Shantz, D. F., Engineering nanospaces: OMS/dendrimer hybrids possessing controllable chemistry and porosity, *Chem. Mater.* **2006,** *18* (13), 2935-2942.
(26) Acosta, E. J.; Carr, C. S.; Simanek, E. E.; Shantz, D. F., Engineering nanospaces: Iterative synthesis of melamine-based dendrimers on amine-functionalized SBA-15 leading to complex hybrids with controllable chemistry and porosity, *Adv. Mater.* **2004,** *16* (12), 985-989.
(27) Sanz, R.; Calleja, G.; Arencibia, A.; Sanz-Perez, E. S., CO_2 capture with pore-expanded MCM-41 silica modified with amino groups by double functionalization, *Micropor. Mesopor. Mat.* **2015,** *209*, 165-171.
(28) Darunte, L. A.; Oetomo, A. D.; Walton, K. S.; Sholl, D. S.; Jones, C. W., Direct air capture of CO_2 using amine functionalized MIL-101(Cr), *ACS Sustain. Chem. Eng.* **2016,** *4* (10), 5761-5768.
(29) McDonald, T. M.; Mason, J. A.; Kong, X. Q.; Bloch, E. D.; Gygi, D.; Dani, A.; Crocella, V.; Giordanino, F.; Odoh, S. O.; Drisdell, W. S.; Vlaisavljevich, B.; Dzubak, A. L.; Poloni, R.; Schnell, S. K.; Planas, N.; Lee, K.; Pascal, T.; Wan, L. W. F.; Prendergast, D.; Neaton, J. B.; Smit, B.; Kortright, J. B.; Gagliardi, L.; Bordiga, S.; Reimer, J. A.; Long, J. R., Cooperative insertion of CO_2 in diamine-appended metal-organic frameworks, *Nature* **2015,** *519* (7543), 303-+.
(30) Shin, S.; Yoo, D. K.; Bae, Y. S.; Jhung, S. H., Polyvinylamine-loaded metal-organic framework MIL-101 for effective and selective CO_2 adsorption under atmospheric or lower pressure, *Chem. Eng. J.* **2020,** *389*.
(31) Gelles, T.; Rezaei, F., Diffusion kinetics of CO_2 in amine-impregnated MIL-101, alumina, and silica adsorbents, *AIChE J.* **2020,** *66* (1).
(32) Wang, X. X.; Fujii, M.; Wang, X. X.; Song, C. S., New approach to enhance CO_2 Capture of "molecular basket" sorbent by using 3-aminopropyltriethoxysilane to reshape fumed silica support, *Ind. Eng. Chem. Res.* **2020,** *59* (15), 7267-7273.

(33) Kumar, P.; Kim, S.; Ida, J.; Guliants, V. V., Polyethyleneimine-modified MCM-48 membranes: Effect of water vapor and feed concentration on N_2/CO_2 selectivity, *Ind. Eng. Chem. Res.* **2008,** *47* (1), 201-208.
(34) McDonald, T. M.; Lee, W. R.; Mason, J. A.; Wiers, B. M.; Hong, C. S.; Long, J. R., Capture of carbon dioxide from air and flue gas in the alkylamine-appended metal-organic framework mmen-Mg-2(dobpdc), *J. Am. Chem. Soc.* **2012,** *134* (16), 7056-7065.
(35) Sakwa-Novak, M. A.; Jones, C. W., Steam induced structural changes of a poly(ethylenimine) impregnated gamma-alumina sorbent for CO_2 extraction from ambient air, *ACS Appl. Mater. Interfaces* **2014,** *6* (12), 9245-9255.
(36) Babu, V. P.; Koros, W. J., The role of polyvinylpyrrolidone in forming open-porous, macrovoid-free mixed matrix sorbents from Torlon(R), a polyamide-imide polymer, *Polym. Eng. Sci.* **2018,** *58* (11), 2106-2114.
(37) Babu, V. P.; Koros, W. J., Fabrication of solution-cast polyacrylonitrile barriers for hollow fiber sorbents used in CO_2 removal from flue gas, *Ind. Eng. Chem. Res.* **2019,** *58* (50), 22561-22568.
(38) Lively, R. P.; Chance, R. R.; Kelley, B. T.; Deckman, H. W.; Drese, J. H.; Jones, C. W.; Koros, W. J., Hollow fiber adsorbents for CO_2 removal from flue gas, *Ind. Eng. Chem. Res.* **2009,** *48* (15), 7314-7324.
(39) Armstrong, M.; Shi, X. Y.; Shan, B. H.; Lackner, K.; Mu, B., Rapid CO_2 capture from ambient air by sorbent-containing porous electrospun fibers made with the solvothermal polymer additive removal technique, *AIChE J.* **2019,** *65* (1), 214-220.
(40) Merkel, T. C.; Zhou, M.; Baker, R. W., Carbon dioxide capture with membranes at an IGCC power plant, *J. Membr. Sci.* **2012,** *389*, 441-450.
(41) Garibay, S. J.; Wang, Z.; Tanabe, K. K.; Cohen, S. M., Postsynthetic modification: A versatile approach toward multifunctional metal-organic frameworks, *Inorg. Chem.* **2009,** *48* (15), 7341-7349.
(42) Sumida, K.; Rogow, D. L.; Mason, J. A.; McDonald, T. M.; Bloch, E. D.; Herm, Z. R.; Bae, T.-H.; Long, J. R., Carbon dioxide capture in metal–organic frameworks, *Chem. Rev.* **2012,** *112* (2), 724-781.
(43) Demessence, A.; D'Alessandro, D. M.; Foo, M. L.; Long, J. R., Strong CO_2 binding in a water-stable, triazolate-bridged metal−organic framework functionalized with ethylenediamine, *J. Am. Chem. Soc.* **2009,** *131* (25), 8784-8786.
(44) Choi, S.; Watanabe, T.; Bae, T.-H.; Sholl, D. S.; Jones, C. W., Modification of the Mg/DOBDC MOF with amines to enhance CO_2 adsorption from ultradilute gases, *J. Phys. Chem. Lett.* **2012,** *3* (9), 1136-1141.
(45) Lee, W. R.; Hwang, S. Y.; Ryu, D. W.; Lim, K. S.; Han, S. S.; Moon, D.; Choi, J.; Hong, C. S., Diamine-functionalized metal–organic framework: exceptionally high CO_2 capacities from ambient air and flue gas, ultrafast CO_2 uptake rate, and adsorption mechanism, *Energy Environ. Sci.* **2014,** *7* (2), 744-751.
(46) Sanz-Pérez, E. S.; Murdock, C. R.; Didas, S. A.; Jones, C. W., Direct capture of CO_2 from ambient air, *Chem. Rev.* **2016,** *116* (19), 11840-11876.
(47) Li, J.-R.; Yu, J.; Lu, W.; Sun, L.-B.; Sculley, J.; Balbuena, P. B.; Zhou, H.-C., Porous materials with pre-designed single-molecule traps for CO_2 selective adsorption, *Nat. Comm.* **2013,** *4* (1), 1538.
(48) Raman, A. P.; Anoma, M. A.; Zhu, L.; Rephaeli, E.; Fan, S., Passive radiative cooling below ambient air temperature under direct sunlight, *Nature* **2014,** *515*, 540.

(49) Fan, S., Thermal photonics and energy applications, *Joule* **2017,** *1* (2), 264-273.
(50) Hossain Md, M.; Gu, M., Radiative cooling: Principles, progress, and potentials, *Adv. Sci.* **2016,** *3* (7), 1500360.
(51) Zhao, B.; Hu, M.; Ao, X.; Chen, N.; Pei, G., Radiative cooling: A review of fundamentals, materials, applications, and prospects, *Appl. Energy* **2019,** *236*, 489-513.
(52) Bhatia, B.; Leroy, A.; Shen, Y.; Zhao, L.; Gianello, M.; Li, D.; Gu, T.; Hu, J.; Soljačić, M.; Wang, E. N., Passive directional sub-ambient daytime radiative cooling, *Nat. Comm.* **2018,** *9* (1), 5001.
(53) Chen, Z.; Zhu, L.; Raman, A.; Fan, S., Radiative cooling to deep sub-freezing temperatures through a 24-h day–night cycle, *Nat. Comm.* **2016,** *7*, 13729.
(54) Gentle Angus, R.; Smith Geoff, B., A subambient open roof surface under the mid-summer sun, *Adv. Sci.* **2015,** *2* (9), 1500119.
(55) Hsu, P.-C.; Liu, C.; Song, A. Y.; Zhang, Z.; Peng, Y.; Xie, J.; Liu, K.; Wu, C.-L.; Catrysse, P. B.; Cai, L.; Zhai, S.; Majumdar, A.; Fan, S.; Cui, Y., A dual-mode textile for human body radiative heating and cooling, *Sci. Adv.* **2017,** *3* (11).
(56) Hsu, P.-C.; Song, A. Y.; Catrysse, P. B.; Liu, C.; Peng, Y.; Xie, J.; Fan, S.; Cui, Y., Radiative human body cooling by nanoporous polyethylene textile, *Science* **2016,** *353* (6303), 1019.
(57) Li, T.; Zhai, Y.; He, S.; Gan, W.; Wei, Z.; Heidarinejad, M.; Dalgo, D.; Mi, R.; Zhao, X.; Song, J.; Dai, J.; Chen, C.; Aili, A.; Vellore, A.; Martini, A.; Yang, R.; Srebric, J.; Yin, X.; Hu, L., A radiative cooling structural material, *Science* **2019,** *364* (6442), 760.
(58) Li, W.; Shi, Y.; Chen, Z.; Fan, S., Photonic thermal management of coloured objects, *Nat. Comm.* **2018,** *9* (1), 4240.
(59) Mandal, J.; Fu, Y.; Overvig, A. C.; Jia, M.; Sun, K.; Shi, N. N.; Zhou, H.; Xiao, X.; Yu, N.; Yang, Y., Hierarchically porous polymer coatings for highly efficient passive daytime radiative cooling, *Science* **2018,** *362* (6412), 315.
(60) Shi, N. N.; Tsai, C.-C.; Camino, F.; Bernard, G. D.; Yu, N.; Wehner, R., Keeping cool: Enhanced optical reflection and radiative heat dissipation in Saharan silver ants, *Science* **2015,** *349* (6245), 298.
(61) Zhai, Y.; Ma, Y.; David, S. N.; Zhao, D.; Lou, R.; Tan, G.; Yang, R.; Yin, X., Scalable-manufactured randomized glass-polymer hybrid metamaterial for daytime radiative cooling, *Science* **2017,** *355* (6329), 1062.
(62) Zhou, L.; Song, H.; Liang, J.; Singer, M.; Zhou, M.; Stegenburgs, E.; Zhang, N.; Xu, C.; Ng, T.; Yu, Z.; Ooi, B.; Gan, Q., A polydimethylsiloxane-coated metal structure for all-day radiative cooling, *Nat. Sustain.* **2019,** *2* (8), 718-724.

Appendix I: State-Point Data for Sorbent Based Systems.

	Units	Measured/ Estimated Performance	Projected Performance
Sorbent			
True Density @ STP	kg/m^3	~1000	~1000
Bulk Density	kg/m^3	~300	~300
Average Particle Diameter	mm	N/A	N/A
Particle Void Fraction	m^3/m^3	N/A	N/A
Packing Density	m^2/m^3	~500	~500
Solid Heat Capacity @ STP	kJ/kg·K	~1.5	~1.5
Crush Strength	kg_f	N/A	N/A
Attrition Index	-	N/A	N/A
Thermal Conductivity	W/(m·K)	~0.26	~0.26
Adsorption			
Pressure	bar	1.01	1.01
Temperature	°C	25	20
Equilibrium Loading	gmol CO_2/kg	1 – 2	2 – 3
Heat of Adsorption	kJ/gmol CO_2	-70	-70
CO_2 Adsorption Kinetics	gmol/time	10 gmol/kg h	50 gmol/kg h
Desorption			
Pressure	bar	1.01	1.01
Temperature	°C	65 – 100	65 – 100
Equilibrium Loading	gmol CO_2/kg	0.2 – 0.4	0.2 – 0.4
Heat of Desorption	kJ/gmol CO_2	-70	-70
CO_2 Desorption Kinetics	gmol/time	20 gmol/kg h	100 gmol/kg h